Journal of Theoretical Biology 486 (2020) 110093

Contents lists available at ScienceDirect

Journal of Theoretical Biology

journal homepage: www.elsevier.com/locate/jtb

Metabolism plays a central role in the cortical spreading depression: Evidence from a mathematical model

G Capo-Rangel[a], L Gerardo-Giorda[a], E Somersalo[a], D Calvetti[b,*]

[a] Basque Center for Applied Mathematics, Spain
[b] Department of Mathematics, Applied Mathematics and Statistics, Case Western Reserve University, Ohio

ARTICLE INFO

Article history:
Received 1 August 2019
Revised 28 October 2019
Accepted 23 November 2019
Available online 26 November 2019

Keywords:
Multiscale modeling
potassium homeostasis
metabolic coupling
brain energetics

ABSTRACT

The slow propagating waves of strong depolarization of neural cells characterizing cortical spreading depression, or depolarization, (SD) are known to break cerebral homeostasis and induce significant hemodynamic and electro-metabolic alterations. Mathematical models of cortical spreading depression found in the literature tend to focus on the changes occurring at the electrophysiological level rather than on the ensuing metabolic changes. In this paper, we propose a novel mathematical model which is able to simulate the coupled electrophysiology and metabolism dynamics of SD events, including the swelling of neurons and astrocytes and the concomitant shrinkage of extracellular space. The simulations show that the metabolic coupling leads to spontaneous repetitions of the SD events, which the electrophysiological model alone is not capable to produce. The model predictions, which corroborate experimental findings from the literature, show a strong disruption in metabolism accompanying each wave of spreading depression in the form of a sharp decrease of glucose and oxygen concentrations, with a simultaneous increase in lactate concentration which, in turn, delays the clearing of excess potassium in extracellular space. Our model suggests that the depletion of glucose and oxygen concentration is more pronounced in astrocyte than neuron, in line with the partitioning of the energetic cost of potassium clearing. The model suggests that the repeated SD events are electro-metabolic oscillations that cannot be explained by the electrophysiology alone. The model highlights the crucial role of astrocytes in cleaning the excess potassium flooding extracellular space during a spreading depression event: further, if the ratio of glial/neuron density increases, the frequency of cortical SD events decreases, and the peak potassium concentration in extracellular space is lower than with equal volume fractions.

1. Introduction

Cortical spreading depolarizations (SD) refer to phenomena characterized by a slowly propagating wave of intense neuronal and glial depolarization, accompanied by temporary suppression of electrical activity and severe failure of ionic homeostasis (Ayata and Lauritzen, 2015; Lourenço et al., 2017). The original description of slowly propagating depolarization waves in cerebral cortex, followed by a suppression of brain activity dates back to the mid 1940s, when Leão (1944) first recorded a spreading suppression of electroencephalographic activity following an electric stimulation on the surface of a rabbit brain. Although subsequently he noticed that a massive wave of excitation was actually preceding the sustained suppression of activity (Leão, 1945), the event had already been named "spreading depression" in the scientific community (Charles and Baca, 2013), and the name stuck. In the following decades, the spreading depolarization was extensively studied, leading gradually to a much better understanding of the underlying mechanisms. A strong stimulus for the research arises from the evidence that SD in humans is related to migraine, and in particular to the visual aura experienced by many migraine patients. Despite the progress in studying SDs, some important questions are still waiting for a definitive answer, including the mechanisms initiating a spreading depolarization, its role in the aura preceding migraine, and the full extent of the consequences of SD events on either normal or injured brain. It is clear that the spreading depolarization involves not only the electrophysiology of the brain but also the metabolism and hemodynamics, and therefore predictive mathematical models suitable to describe the changes in brain's metabolic activity and cerebral blood flow at the onset, during, and following SD events may shed light on the feedback and feedforward mechanisms related to the phenomenon.

* Corresponding author
E-mail addresses: dxc57@case.edu, daniela.calvetti@case.edu (D. Calvetti).

https://doi.org/10.1016/j.jtbi.2019.110093
0022-5193/

Experimental results reported in the literature indicate that the ways in which the brain reacts to SD events may vary quite widely and depend on its state at the onset. Under normoxic conditions, an SD event is a reversible process that does not cause neuronal damage (Seidel et al., 2016; Nedergaard and Hansen, 1988; Lian and Stringer, 2004; Takano and Nedergaard, 2009) and, in fact, its potential protective role against future ischemic events has been recently discussed in the experimental literature (Takano and Nedergaard, 2009; Nedergaard and Hansen, 1993; Horiguchi et al., 2005; Busija et al., 2008). In an acutely injured brain, however, SDs can severely slow down the recovery process or even cause secondary brain damage (Ayata and Lauritzen, 2015; Lauritzen et al., 2011; Balança et al., 2017; Feuerstein et al., 2010; Rogers et al., 2013). SD waves, known to occur spontaneously after severe head trauma in ischemic or hypoxic brain tissue (Lauritzen et al., 2011), can also be triggered in normoxic brain through various electrical, mechanical or chemical stimuli (Somjen, 2001; Dalkara et al., 2006): with a stimulus strong enough to focally increase extracellular potassium concentration in excess of 10 to 12 mM, a slow propagating wave may be initiated (Ayata and Lauritzen, 2015; Takano and Nedergaard, 2009). As the wave travels across the cortex, it is accompanied by a large increase in extracellular potassium, intracellular sodium and intracellular chloride concentrations (Ayata and Lauritzen, 2015; Takano and Nedergaard, 2009; Nedergaard and Hansen, 1993; Somjen, 2001), leading to accumulation of water, cell swelling and pronounced shrinkage of the extracellular space (Ayata and Lauritzen, 2015; Takano et al., 2007). The local pressure increase may be coupled to reduced cerebral blood flow.

In part, due to the inherently electrophysiological manifestation of SD events, most of the attention has focused on the changes in the electrical activity of the brain, although some investigators have also looked at how the cerebral hemodynamics and metabolism are affected during and following the passing of SD waves. As restoration of the ionic gradients has one of the largest observed metabolic costs in brain (Ayata and Lauritzen, 2015; Seidel et al., 2016), SDs have been shown to cause substantial increase in both aerobic and anaerobic metabolism (Ayata and Lauritzen, 2015), with significant (50%) depletion of ATP concentration (Mies and Paschen, 1984; Selman et al., 2004). The typical metabolic signature of an SD event is a considerable decrease in extracellular glucose and a large increase in extracellular lactate concentration (Ayata and Lauritzen, 2015; Balança et al., 2017; Mies and Paschen, 1984; Feuerstein et al., 2016). Higher rates of oxidative phosphorylation and an increased oxygen demand during SD were reported in the literature (Fordsmann et al., 2013; Galeffi et al., 2011). Likewise, substantial increases in cerebral metabolic rates of oxygen and glucose were also detected (Ayata and Lauritzen, 2015; Seidel et al., 2016; Balança et al., 2017; Feuerstein et al., 2016; Adachi et al., 1995).

Experimental investigations of multiple SD waves reported cumulative changes in the concentration of metabolites (Feuerstein et al., 2016; Hashemi et al., 2009). Feuerstein et al. (2016) noticed a stepwise decay of extracellular glucose and increase in extracellular lactate concentrations with each passing SD wave. Similar behavior is observed for the concentration of oxygen, which is reported to be decreasing stepwise in the case of recurrent SDs under pathologic conditions (Bosche et al., 2010; Dreier et al., 2009). In light of these observations, cortical SD is believed to cause progressive hypoxia, ischemia and acute metabolic damage in human subjects with brain injury (Seidel et al., 2016; Carlson et al., 2012).

In healthy brain, cerebral hemodynamic response to increased metabolic demand of an SD event is an extreme initial hyperemia, with CBF rising 100–250% over baseline value 15 to 20 seconds after the onset of the ictal DC shift (Ayata and Lauritzen, 2015; Lourenço et al., 2017; Lauritzen et al., 2011; Balança et al., 2017; Mies and Paschen, 1984; Feuerstein et al., 2016) and persisting approximately 1 to 3 min (Ayata and Lauritzen, 2015; Lauritzen et al., 2011; Hadjikhani et al., 2001). Once the hyperemia ends, the blood flow either stabilizes 20–30% below baseline value for at least one hour (Ayata and Lauritzen, 2015; Takano and Nedergaard, 2009; Lauritzen et al., 2011; Hadjikhani et al., 2001) or returns to its baseline value (Lourenço et al., 2017). Note that the cerebral blood flow response varies substantially between different species (Ayata and Lauritzen, 2015; Busija et al., 2008; Ayata et al., 2004). While most studies on rats, cats, monkeys and humans capture the behavior described above, measurements performed on mice follow a totally different pattern: no initial hyperemia was detected, instead the blood flow presented a fast decrease to about 40% of the baseline CBF (Ayata et al., 2004). Other factors that must be taken into account when studying the vascular response are the type of anesthesia used in the experiment (Masamoto and Kanno, 2012; Kudo et al., 2008) and the way in which the SD was triggered (Busija et al., 2008).

Because of the similarities between the spreading of depression waves and migraine aura, already noticed by Leão (1945), a causal relation between the two has been hypothesized (Charles and Baca, 2013), although there is only very faint electrophysiological evidence for the claim (Lauritzen M and J, 1981), and a definitive explanation of the relation between the two is still missing.

While experimental observations point to an important role of metabolism in SD events and suggest that understanding how metabolic processes change in connection with CSD may be a way to get a handle on them, a mathematical model capable of simulating the electrophysiological and metabolic changes of the brain induced by SD waves is the tool needed for the task, in particular, to test the viability of different hypotheses about the mechanism underneath SD event as well as the interplay between the two regimes. In this paper we propose a new computational predictive model for the study of the SD, integrating electrophysiology and metabolism in a human neurovascular unit comprising neuron, astrocyte, extracellular space, and a arterial-venous blood compartments. The model, following the original formulation in Calvetti et al. (2018), includes a two-way feedback process linking electrophysiology and metabolism. As a novel feature, the electrophysiology module in this work is based on the extended model of Hübel et al. (2017) that is capable to deal with the large ionic gradients characteristic to SD events, and to follow in detail the electrolyte dynamics during the event. The blood flow is prescribed as input variable, rather than determined by the electro-metabolic state of the unit as in Capo Rangel et al. (2019), because it has been observed experimentally that SD events affect the hemodynamics of the brain in a yet unclear manner, and therefore postulating a feedback mechanism could be misleading. In light of the observed swelling of astrocytes and concomitant shrinkage of extracellular space during a SD event, the model has been modified so as to allow the relative volume fractions of the compartments to change dynamically. The model is capable of reproducing series of SD events, with the metabolic responses matching with the experimental observations. One of the most important findings is that without the metabolic coupling, the electrophysiology model alone is not capable to reproduce spontaneous repeated CD events, underlining the central role of metabolism in understanding the phenomenon. Furthermore, the model supports the hypothesis that when the volume fraction of astrocytes increases, the frequency and intensity of CSD waves decreases, as illustrated in one of the computed experiments, in agreement with the conclusions in Seidel et al. (2016); Fujita et al. (2015), which were partly motivated by the recent observation Fujita et al. (2015) that regions in the brain characterized by larger number of glial cells, in particular astrocytes, are more resistant to SD episodes.

Before describing the model in full detail, a few considerations about how to reconcile the use of a spatially lumped model to

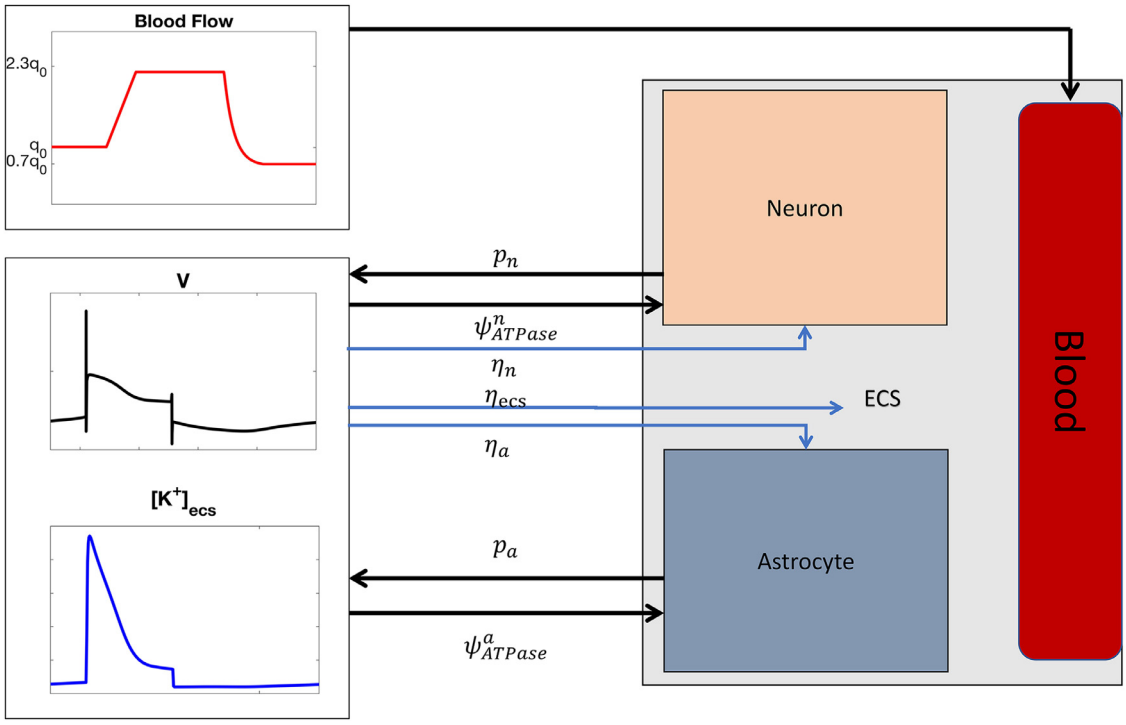

Fig. 1. Schematic overview of the double feedback coupling mechanism between the electrophysiology and metabolism of a neuron-astrocyte complex during SD simulation. The panel in the left upper corner shows the blood flow protocol during a SD event, characterized by a strong hyperemia, followed by a mild vasoconstriction to 70% of the cerebral blood flow baseline value. The CBF is an input to the metabolic model, which consists of four compartments: neuron, astrocyte, extracellular space and blood. The middle left panel displays the typical change of the membrane potential during a SD episode and the bottom left panel shows the rise in the concentration of extracellular potassium. The energetic demand to support the restoration of ionic homeostasis is embedded in the metabolic model via the ATPase fluxes denoted by ψ^n_{ATPase} and ψ^a_{ATPase}, together with the change in morphology of the cells captured by the volume fractions η_n, η_a, and η_{ecs}. Conditioned on the availability of the different metabolites, the metabolic model produces a certain amount of energy expressed in terms of the phosphorylation states p_n and p_a, which are fed back into the electrophysiological model.

study SD events characterized by the spreading of depolarization waves are in order. Our model is based on the assumption that a reference volume of one gram tissue is the aggregate of spatially homogenous compartments, each contributing according to its relative volume fraction. In the following, terms like neuron and astrocyte will be used to refer to the averaged contribution of the neurons, or astrocytes, weighted according to their relative volume fractions, not to individuals cells. For a more extensive discussion on how to interpret compartments in a spatially lumped model as well as for scaling of reaction fluxes and transports, we refer to Capo Rangel et al. (2019). As pointed out in the cited article, interfacing different scales at which metabolic and electrophysiological processes occur is a challenging problem, and in our model it was solved by adjusting the latter so as to correspond to the activity of a one gram tissue of gray matter. Another point that needs elucidation in our model is how sustained high activation periods should be understood: as explained in Capo Rangel et al. (2019), the firing at given frequency over a period is not intended as describing the state of single neurons, rather, the firing rate represents the average rate over the aggregate of the neurons in the volume. The current model does not include the spatial dynamics of the SD events, and should therefore be viewed as a window on the brain from which we observe local changes in electrophysiology and metabolism as SD waves pass by. The extension to a spatially distributed model is beyond the scope of this paper.

2. Materials and methods

We propose a double feedback model integrating electrical activity and metabolism of a neuron-astrocyte complex specifically tailored for following changes in brain in connection with cortical spreading depolarization. The underlying model, that extends one originally proposed in Calvetti et al. (2018), addresses the computational challenges due to different orders of magnitude of the time scales of electrophysiological and metabolic processes. For this study, the original model was modified to allow the volume fractions to change in time to account for the swelling of neurons and astrocytes and the resulting shrinkage of the extracellular space. A sketch of the main mechanisms underlying the coupling of the electrophysiology and metabolism in the case of SD is shown in Fig. 1.

2.1. Metabolic model

The metabolism of a neuron-astrocyte complex is described through a lumped four compartment model comprising two cellular compartments: neuron (n) and astrocyte (a), extracellular space (ecs), and blood compartment (b). Each compartment occupies a volume fraction $\eta(t) = \{\eta_n(t), \eta_a(t), \eta_{\text{ecs}}(t), \eta_b(t)\}$, which changes over time to account for morphologic alterations characteristic to depolarization waves. The parameters and time scales of this model, originally proposed in Calvetti and Somersalo (2011), were previously calibrated for a volume of one gram of tissue of gray matter (Calvetti et al., 2018; Calvetti and Somersalo, 2011).

The metabolic model follows the time courses of the metabolites in the four compartments: glucose, lactate and oxygen concentrations are tracked in all four compartments, and those of ATP, ADP, pyruvate, phosphocreatine, creatine, NAD^+ and NADH in the two cellular compartments. We collect all concentrations in the four compartments into the vector $[M](t)$,

$$[M](t) = [[M]_b(t); [M]_{\text{ecs}}(t); [M]_n(t); [M]_a(t)].$$

Neuron and astrocyte compartments exchange metabolites through the extracellular space, which in turn communicates with

the blood compartment through the Blood Brain Barrier. Therefore, the changes in glucose, lactate and oxygen concentrations depend on the transport fluxes between ecs and neuron, ecs and astrocyte, and between ecs and blood domain. Finally, glucose, lactate and oxygen concentrations in blood compartment depend on the rates at which the metabolites are exchanged between blood and ecs as well as on the blood flow $q(t)$.

In neuron and astrocyte, biochemical reactions produce or consume ATP and their reaction fluxes are modeled according to Michaelis-Menten type kinetics. A complete list of the biochemical reactions and the mathematical expressions of the corresponding fluxes can be found in the literature (Calvetti et al., 2018; Calvetti and Somersalo, 2011; Capo Rangel et al., 2019). The coupling between metabolism and electrophysiological activity is based on ATP production and consumption; for future reference, we denote phosphorylation and redox states by

$$p_c = \frac{[\mathrm{ATP}]_c}{[\mathrm{ADP}]_c}, \quad r_c = \frac{[\mathrm{NADH}]_c}{[\mathrm{NAD}^+]_c}, \quad \text{for } c = \{n, a\}. \tag{1}$$

ATP dephosphorylation, which releases energy at rate $E = 30.5$ kJ/mol, is used to satisfy the energetic requirements of the sodium-potassium pump in neuron, potassium glial cleaning, and various unspecified household tasks. ATP dephosphorylation reaction rates in neuron and astrocyte, denoted by ψ^n_{ATPase} and ψ^a_{ATPase}, are modeled as

$$\psi^n_{\mathrm{ATPase}} = H_n + s\eta_n E[I_{\mathrm{pump}}], \tag{2}$$

$$\psi^a_{\mathrm{ATPase}} = H_a + s\frac{\eta_{\mathrm{ecs}}}{2} E[I_{\mathrm{glia}}], \tag{3}$$

where H_n and H_a account for unspecified energetic cost in the two cells. Here the ion mass current $E[I_{\mathrm{pump}}]$ represents the energetic cost for the sodium-potassium pump, $E[I_{\mathrm{glia}}]$ the energetic cost of glial potassium cleaning, both expressed in units of mM/s, η_n is the volume fraction of the neuron, η_{ecs} is the volume fraction of the ecs, and s is a proportionality constant which allows us to compensate for the different volumes assumed in our model. The differential equations describing the metabolic model can be summarized as

$$\frac{d[M]}{dt} = F\big([M], [M]_{\mathrm{art}}, \psi^n_{\mathrm{ATPase}}, \psi^a_{\mathrm{ATPase}}, q, \eta_n, \eta_{\mathrm{ecs}}, \eta_a\big), \tag{4}$$

where the entries of the vector $[M]$ are the concentrations of the 26 metabolites, and those of $[M]_{\mathrm{art}}$ the arterial concentrations of glucose, lactate and oxygen (see Table 1), q is the blood flow, and η_n, η_{ecs} and η_a are the volume fractions of neuron, ecs, and astrocyte compartments, respectively.

2.2. Electrophysiologic model

Our starting point for describing the brain electrical activity is the model by Hübel et al. (2017) which was specifically designed to account for the massive changes in ionic concentrations during the passing of depolarization waves. This model, unlike others (Cressman et al., 2009; Barreto and Cressman, 2011; Hübel and Dahlem, 2014; Wei et al., 2014), adheres to the principle of electroneutrality and mass conservation, and it includes glutamate dynamics accounting for the morphologic changes occurring during cortical spreading depression.

The rate equations for describing the membrane potential and gate dynamics are built on the Hodgkin-Huxley model as

$$\tau\frac{dV}{dt} = -\frac{1}{C}\big(I_{\mathrm{Na}^+} + I_{\mathrm{K}^+} + I_{\mathrm{Cl}^-} + I_{\mathrm{pump}}\big), \tag{5}$$

$$\tau\frac{dw}{dt} = \varphi(\alpha_w(V)(1-w) - \beta_w(V)w), \quad w \in \{h, n\}, \tag{6}$$

where C is the capacitance of the neuronal membrane, V is the membrane potential, n and h are the activation gates for sodium and potassium, α_w and β_w are voltage saturation functions, $\tau = 10^3$ is a conversion factor, and φ is a time constant. The voltage dependent ionic currents of sodium (I_{Na^+}), potassium (I_{K^+}), and chloride (I_{Cl^-}), are expressed in terms of the sodium, potassium and chloride conductances (g_{Na^+}, g_{K^+} and g_{Cl^-}, respectively) and the corresponding leak conductances ($g_{\mathrm{Na}^+,\mathrm{leak}}$, $g_{\mathrm{K}^+,\mathrm{leak}}$) listed in Table 1, as

$$\begin{aligned}
I_{\mathrm{Na}^+} &= g_{\mathrm{Na}^+} m^3 h(V - V_{\mathrm{Na}^+}) + g_{\mathrm{Na}^+,\mathrm{leak}}(V - V_{\mathrm{Na}^+}) + I^{\mathrm{NMDA}}_{\mathrm{Na}^+} + I^{\mathrm{AMPA}}_{\mathrm{Na}^+} + I^{\mathrm{co}}_{\mathrm{Na}^+},\\
I_{\mathrm{K}^+} &= g_{\mathrm{K}^+} n^4(V - V_{\mathrm{K}^+}) + g_{\mathrm{K}^+,\mathrm{leak}}(V - V_{\mathrm{K}^+}) + I^{\mathrm{NMDA}}_{\mathrm{K}^+} + I^{\mathrm{AMPA}}_{\mathrm{K}^+} + I^{\mathrm{co}}_{\mathrm{K}^+},\\
I_{\mathrm{Cl}^-} &= g_{\mathrm{Cl}^-}(V - V_{\mathrm{Cl}^-}) + I^{\mathrm{co}}_{\mathrm{Cl}^-},
\end{aligned}$$

Here, m is the gate for sodium inactivation modeled, as in Cressman et al. (2009) and Barreto and Cressman (2011), through the adiabatic approximation,

$$m = \frac{\alpha_m}{\alpha_m + \beta_m}.$$

The discussion of currents corresponding to the NMDA receptors ($I^{\mathrm{NMDA}}_{\mathrm{Na}^+}$ and $I^{\mathrm{NMDA}}_{\mathrm{K}^+}$) and AMPA receptors ($I^{\mathrm{AMPA}}_{\mathrm{Na}^+}$ and $I^{\mathrm{AMPA}}_{\mathrm{K}^+}$) is postponed to when glutamate dynamics is addressed. The reversal potentials for sodium, potassium and chloride are given by the Nernst equation,

$$V_x = \frac{26.64}{z_x}\ln\left(\frac{x_{\mathrm{ecs}}}{x_i}\right), \text{ where } \quad x = \{\mathrm{Na}^+, \mathrm{K}^+, \mathrm{Cl}^-\} \tag{7}$$

where z_x is the valence of each ion x.

While earlier models (Cressman et al., 2009; Barreto and Cressman, 2011) only followed the concentrations of sodium and potassium, Hübel et al. (2017) track also the concentration of chloride, accounting separately for these ions in intracellular space (i), extracellular space (ecs) and glia (g) compartments, whose volume fractions are ω_i, ω_{ecs} and ω_g, respectively. The differential equations governing the dynamics of intracellular potassium and

Table 1
Parameters in the coupled electro-metabolic CSD model.

Electrophysiological model

Symbol	Value	Unit	Symbol	Value	Unit
g_{Na^+}	100	mS/cm^2	α_{AMPA}	1.1	mM msec
g_{K^+}	40	mS/cm^2	β_{AMPA}	0.19	1/msec
g_{Cl^-}	0.05	mS/cm^2	α_{NMDA}	0.072	mM msec
$g_{\mathrm{Na}^+,\mathrm{leak}}$	0.0135	mS/cm^2	β_{NMDA}	0.0066	1/msec
$g_{\mathrm{K}^+,\mathrm{leak}}$	0.05	mS/cm^2	g_{AMPA}	0.486	mS/cm^2
c_m	1	1/msec	g_{NMDA}	0.139	mS/cm^2
φ	3	1/msec	$\nu^{\max}_{c\to i}$	0.03	mM/sec
F	97,485	C/mol	$[\mathrm{Mg}^{2+}]$	1.2	mM
A_m	18,000	μm^2	N_{syn}	5000	–
μ_{pump}	0.1	–	s	82,500	–
μ_{glia}	0.1	–	Protocol A		
ρ	6.46	μA/cm^2	ω^0_i	7500	μm^3
λ	1e–4	1/msec	ω^0_g	7500	μm^3
λ_{rel}	5e–3	mM/msec	ω^0_{ecs}	2500	μm^3
G_{glia}	1.6e–2	mM/msec			
K_{bath}	12	mM	Protocol B		
$\Delta K^{\max}_{\mathrm{glia}}$	350	fmol	ω^0_i	5000	μm^3
X_i	5	mM	ω^0_g	10,000	μm^3
X_{ecs}	19	mM	ω^0_{ecs}	2500	μm^3
A_i	146	mM			
A_{ecs}	18	mM			
N^0_g	315	fmol			

Metabolic model

Symbol	Value	Unit
$[\mathrm{Glc}]_{\mathrm{art}}$	5	mM
$[\mathrm{Lac}]_{\mathrm{art}}$	1.1	mM
$[\mathrm{O}_2]_{\mathrm{art}}$	9.14	mM
η_b	0.04	–
H_n	4.30	mM/min
H_a	3.58	mM/min

Blood flow

Symbol	Value	Unit
t_1	126	sec
t_d	20	sec
t_{r1}	30	sec
t_{r2}	40	sec
α	0.1	sec
q_0	0.4	mL/min

chloride in neuron are

$$\tau^2 \frac{d[K^+]_i}{dt} = -\gamma\,(I_{K^+} - 2I_{\text{pump}}), \tag{8}$$

$$\tau^2 \frac{d[Cl^-]_i}{dt} = \gamma I_{Cl^-}, \tag{9}$$

where $\gamma = A_m/(10\,F)$ is the conversion parameter of the current expressed in $\mu A/cm^2$ to units of fmol/s, proportional to the ratio between membrane surface area (A_m) and Faraday constant (F).

The ionic current induced by the sodium potassium pump is given by

$$I_{\text{pump}} = \left(\frac{\rho_{\text{pump}}}{1+\exp((15-[Na^+]_i)/3)}\right) \times \left(\frac{1}{1+\exp(5.5-[K^+]_{\text{ecs}})}\right), \tag{10}$$

where ρ_{pump} is the strength of the pump.

To guarantee electroneutrality of the model, Hübel et al. (2017) include a condition for conservation of intracellular charge, that is, $[Na^+]_i + [K^+]_i + [Cl^-]_i = [Na^+]_i^0 + [K^+]_i^0 + [Cl^-]_i^0$, where the superscript (0) refers to the initial concentrations. We solve the balance equation for the intracellular sodium concentration,

$$[Na^+]_i = [Na^+]_i^0 + [K^+]_i^0 + [Cl^-]_i^0, -[K^+]_i - [Cl^-]_i. \tag{11}$$

According to the mass conservation principle obeyed by the model, the sum of ions in intracellular and extracellular space is constant, hence the extracellular concentrations of sodium, potassium and chloride can be computed according to the formulas

$$[Na^+]_{\text{ecs}} = [Na^+]_{\text{ecs}}^0 + [Na^+]_i^0 - [Na^+]_i - \Delta Na_{\text{glia}}, \tag{12}$$

$$[K^+]_{\text{ecs}} = [K^+]_{\text{ecs}}^0 + [K^+]_i^0 - [K^+]_i - \Delta K_{\text{glia}} - \Delta K_{\text{bath}}, \tag{13}$$

$$[Cl^-]_{\text{ecs}} = [Cl^-]_{\text{ecs}}^0 + [Cl^-]_i^0 - [Cl^-]_i - \Delta Cl_{\text{glia}}. \tag{14}$$

where ΔK_{glia} and ΔK_{bath} indicate the ionic exchange with glia cell and external potassium bath, respectively, and the fluxes of chloride and sodium in glia are not explicitly modeled, but are approximated Hübel et al. (2017) as

$$\Delta Na_{\text{glia}} = -0.2\Delta K_{\text{glia}}, \quad \Delta Cl_{\text{glia}} = 0.8\Delta K_{\text{glia}}.$$

Recent papers (Hübel et al., 2017; Hübel and Dahlem, 2014; Hübel and Ullah, 2016; Hübel et al., 2016) have stressed the crucial role of astrocyte in clearing excess potassium that floods extracellular space during an SD event. While in previous models the potassium clearing was attributed only to the coupling with an extracellular bath of potassium (Hübel and Ullah, 2016) or glial potassium buffering (Hübel et al., 2016), the current model includes all the above mechanisms.

The expression for the rate of ionic exchange with the glia is given by

$$\tau^2 \frac{d\Delta K_{\text{glia}}}{dt} = I_{\text{glia}}\,\omega_{\text{ecs}}, \tag{15}$$

where the glial uptake is modeled as

$$I_{\text{glia}} = -\lambda_{\text{rel}} + \frac{G_{\text{glia}}}{1+\exp\left(\frac{5.5-[K^+]_{\text{ecs}}}{2.5}\right)} \frac{\Delta K_{\text{glia}}^{\max} - \Delta K_{\text{glia}}}{\Delta K_{\text{glia}}^{\max}}, \tag{16}$$

λ_{rel} being the constant release rate, $\Delta K_{\text{glia}}^{\max}$ maximum potassium uptake rate and G_{glia} the strength of glial uptake.

Similarly, the diffusive coupling to the bath is governed by the equation

$$\tau^2 \frac{d\Delta K_{\text{bath}}}{dt} = I_{\text{diff}}\,\omega_{\text{ecs}}, \tag{17}$$

where the diffusion current is

$$I_{\text{diff}} = \lambda([K]_{\text{ecs}} - K_{\text{bath}}),$$

λ is a diffusion coefficient, and K_{bath} is the bath potassium concentration, which in our computed experiments is interpreted broadly as an extended source of potassium, accounting for the SD activity in the surrounding tissue, and set to 12 mM. In the current model, the elevated ambient potassium concentration is the trigger of the SD event. Elevated potassium level is commonly used both in experimental and computational literature to trigger the SD, see, e.g., Spong and Robertson (2016), Cozzolino et al. (2018), Wei et al. (2014), Hübel et al. (2017) and Florence et al. (2009).

The large swelling typical of neurons and astrocytes during cortical spreading depression, believed to be osmosis driven, causes a change in cellular volumes. To maintain the balance between the soma, glia and extracellular space, following Hübel et al. (2017), osmotic equilibrium is modeled as

$$\frac{N_i}{\omega_i} = \frac{N_{\text{ecs}}}{\omega_{\text{ecs}}} = \frac{N_g}{\omega_g} = \frac{N_{\text{tot}}}{\omega_{\text{tot}}}, \tag{18}$$

where N_i, N_{ecs} and N_g are the total number of intracellular, extracellular and glial ions, anions ($A_{i/\text{ecs}}$) and neutral matter ($X_{i/\text{ecs}}$), given by

$$N_i = [Na^+]_i + [K^+]_i + [Cl^-]_i + A_i + X_i \tag{19}$$

$$N_{\text{ecs}} = [Na^+]_{\text{ecs}} + [K^+]_{\text{ecs}} + [Cl^-]_{\text{ecs}} + A_{\text{ecs}} + X_{\text{ecs}} \tag{20}$$

$$N_g = N_g^0 + \Delta Na_{\text{glia}} + \Delta K_{\text{glia}} + \Delta Cl_{\text{glia}}, \tag{21}$$

and N_g^0 is chosen so as to balance the glial cell and extracellular space (Hübel et al., 2017). The volume changes in the three compartments is computed from the osmotic equilibrium expressed by the equation

$$\omega_j = N_j \frac{\omega_{\text{tot}}}{N_{\text{tot}}} \quad \text{with} \quad j = \{i,\ \text{ecs},\ g\}, \tag{22}$$

where $N_{\text{tot}} = N_i + N_{\text{ecs}} + N_g$ and $\omega_{\text{tot}} = \omega_i + \omega_{\text{ecs}} + \omega_g$.

In the model by Hübel et al. (2017) a large immediate increase in glutamate level at the onset of a spreading depolarization is included, which was not part of earlier models of brain electrical activity (Cressman et al., 2009; Barreto and Cressman, 2011; Hübel and Dahlem, 2014; Hübel and Ullah, 2016; Hübel et al., 2016; Ullah et al., 2015). Glutamate, the main excitatory neurotransmitter in brain, when present in large amounts, binds to AMPA and NMDA receptors, which, once activated, trigger the release of more glutamate and potassium whose diffusion to nearby cells contributes to the propagation of the depolarization wave. The gating functions of NMDA and AMPA, denoted by r_{NMDA}, r_{AMPA}, are modeled according to Hodgkin-Huxley formalism,

$$\tau \frac{dr_{\text{AMPA}}}{dt} = [Gl]_c \alpha_{\text{AMPA}}(1 - r_{\text{AMPA}}) - \beta_{\text{AMPA}} r_{\text{AMPA}}, \tag{23}$$

$$\tau \frac{dr_{\text{NMDA}}}{dt} = [Gl]_c \alpha_{\text{NMDA}}(1 - r_{\text{NMDA}}) - \beta_{\text{NMDA}} r_{\text{NMDA}}. \tag{24}$$

where $[Gl]_c$ denotes the concentration of glutamate in the cleft, to emphasize the fact that the opening of the channels occurs when this neurotransmitter is present in large amounts, and $\alpha_{\text{AMPA/NMDA}}$, $\beta_{\text{AMPA/NMDA}}$ are gating constants for the AMPA and NMDA receptors. The AMPA currents are modeled as

$$I_{Na^+/K^+}^{\text{AMPA}} = g_{\text{AMPA}} r_{\text{AMPA}}(V - V_{Na^+/K^+}), \tag{25}$$

g_{AMPA} denoting the conductance of the AMPA channels, while the NMDA currents are given by

$$I_{Na^+/Na^+}^{\text{NMDA}} = g_{\text{NMDA}} r_{\text{NMDA}} \frac{V - V_{Na^+/K^+}}{1 + 0.33[Mg^{2+}]\exp(-0.07V - 0.7)}, \tag{26}$$

where g_{NMDA} is the conductance of NMDA channels and $[Mg^{2+}]$ denotes the magnesium concentration, assumed constant. Since each molecule of glutamate is co-transported with three ions of sodium

and one ion of chloride in exchange for the release of one potassium ion, we express the co-transport currents of sodium, potassium and chloride as

$$I^{co}_{Na^+} = \frac{3}{\gamma}\left(\nu^{max}_{c\to i}\frac{[Gl]_c}{[Gl]_c+K_m}\omega_{en}N_{syn} + \nu^{max}_{ecs\to i}\frac{[Gl]_{ecs}}{[Gl]_{ecs}+K_m}\omega_{ecs}\right), \quad (27)$$

$$I^{co}_{K^+} = -\frac{1}{\gamma}\left(\nu^{max}_{c\to i}\frac{[Gl]_c}{[Gl]_c+K_m}\omega_{en}N_{syn} + \nu^{max}_{ecs\to i}\frac{[Gl]_{ecs}}{[Gl]_{ecs}+K_m}\omega_{ecs}\right), \quad (28)$$

$$I^{co}_{Cl^-} = -\frac{1}{\gamma}\left(\nu^{max}_{c\to i}\frac{[Gl]_c}{[Gl]_c+K_m}\omega_{en}N_{syn} + \nu^{max}_{ecs\to i}\frac{[Gl]_{ecs}}{[Gl]_{ecs}+K_m}\omega_{ecs}\right). \quad (29)$$

Above, $\nu^{max}_{c\to i}$ is the maximum uptake velocity from the cleft to the neuron, assumed constant, K_m is the affinity constant of the uptake system, N_{syn} is the number of synapses activated during the SD event, and ω_{en} is the volume inside the glial envelope. The corresponding values are listed in Table 1. A complete description of the model for mechanisms controlling glutamate release can be found in the literature (Hübel et al., 2017).

To account for the metabolic response to an SD event, we express the current contribution from the sodium potassium pump and glial uptake as

$$I_{pump} = \frac{p_n}{p_n+\mu_{pump}}\left(\frac{\rho}{1+\exp((15-[Na^+]_i)/3)}\right) \times\left(\frac{1}{1+\exp(5.5-[K^+]_{ecs})}\right),$$

$$I_{glia} = \frac{p_a}{p_a+\mu_{glia}}\left[-\lambda_{rel}+G_{glia}\left(1+\exp\left(\frac{5.5-[K^+]_{ecs}}{2.5}\right)\right)^{-1} \times\frac{\Delta K^{max}_{glia}-\Delta K_{glia}}{\Delta K^{max}_{glia}}\right],$$

where μ_{pump} and μ_{glia} are affinity constants, p_n and p_a are the phosphorylation states for neuron and astrocyte defined in (1). As proposed by Calvetti et al. (2018), the phosphorylation dependent terms constitute the metabolic feedback into the electrophysiology model.

In summary, the electrophysiology model is governed by a system of 17 differential equations: collecting the components in a vector u, we can write the system formally as

$$\frac{du}{dt} = f(u, p_n, p_a, \omega_i, \omega_{ecs}, \omega_g), \quad (30)$$

to emphasize the dependency of u on the phosphorylation rates p_n, p_a and the volumes ω_i, ω_{ecs} and ω_g of the neuron, extracellular space and glia. To interface with the metabolic model, we introduce dimensionless volume fractions,

$$\eta_n = \frac{\omega_n}{\omega_{tot}}, \quad \eta_g = \frac{\omega_g}{\omega_{tot}}, \quad \eta_{ecs} = \frac{\omega_{ecs}}{\omega_{tot}}, \quad (31)$$

where $\omega_{tot} = \omega_n + \omega_g + \omega_{ecs}$ is the total volume. For consistency with the scale units used in the metabolic model, the sodium-potassium current and the glial uptake current must be expressed in units of mM/sec,

$$E[I_{pump}] = \frac{\gamma}{\omega_i\tau}I_{pump}, \quad E[I_{glia}] = \frac{1}{\tau}I_{glia}. \quad (32)$$

Coupling (4) and (30), we arrive at a double feedback model governed by a system of 43 differential equations. The input to the electro-metabolic SD model consists of arterial concentrations of glucose, lactate and oxygen ($[M]_{art}$) and cerebral blood flow $q(t)$. The main principles behind the feedback mechanism are that:

- The metabolic model determines the phosphorylation states in neuron and astrocyte, which constitute the input for the electrophysiology model;
- The electrophysiology model dictates the energetic demand in neuron and astrocyte, which, together with the volume changes, are inputs of the metabolic model.

While a model with a double feedback mechanism linking electrophysiology and metabolism in brain was already proposed in Calvetti et al. (2018) to elucidate how brain electric activity depends on and affects metabolism under normal circumstances, the main novelty of the present model is the incorporation of the extended model by Hübel et al. (2017) with proper metabolic coupling to address the extreme conditions accompanying cortical SD waves, comprising large electrolyte gradients and changes in the relative volume fractions of the cell compartments and extracellular space, as well as the effect of glutamate to the electrolyte fluxes.

3. Simulation protocols

All computed experiments with the coupled electro-metabolic SD model were performed using the Matlab software. The time interval for each protocol was set to 30 min, and we set k_{bath} = 12 mM, large enough to trigger various depolarization waves, representing the anomalous ambient conditions during the SD event. Two separate protocols were considered: in the first one, referred to as Protocol A, the volume fractions of neuron and astrocyte are equal, while in the second one, referred to as Protocol B, the volume fraction of the astrocyte is twice that of the neuron. The volumes corresponding to Protocol A and Protocol B are given in Table 1. Protocol B, motivated by the recent literature, highlights the important role of the glial cells, especially their buffering of extracellular potassium, uptake of neurotransmitters released by the excitatory synapses, and mediating the vascular response (Seidel et al., 2016; Filosa et al., 2016; Cozzolino et al., 2018; Attwell et al., 2010). Consequently, we expect that brain regions characterized by an increased number of glial cells, may be either refractory to SD, or reduce its propagation velocity (Seidel et al., 2016; Fujita et al., 2015; Karunasinghe and Lipski, 2013). The blood flow profile for both protocols has been designed to mimic the cerebral blood flow response to SD reported in experimental literature. Under normal physiologic conditions, the neuronal silencing characteristic to cortical SD is often accompanied by an initial very large increase in the cerebral blood flow, reported to be in the range from 100% (Selman et al., 2004; Feuerstein et al., 2016) to 130%, (Lourenço et al., 2017; Lauritzen et al., 2011; Balança et al., 2017), and even up to 200% (Piilgaard and Lauritzen, 2009) above the baseline. The hyperemia, which occurs with a delay of 15 to 20 seconds in response to the extremely high energy demand at the onset of the episode (Ayata and Lauritzen, 2015), can be sustained only for a short period of 1 to 2 min (Ayata and Lauritzen, 2015; Lauritzen et al., 2011) and is followed by one to two hours of constant blood flow at baseline or 20–30% below it (Takano and Nedergaard, 2009; Lauritzen et al., 2011; Hadjikhani et al., 2001). Another proposed hemodynamic response to the SD comprises a brief vasoconstriction preceding the depolarization waves (Lauritzen et al., 2011), although the experimental literature (Seidel et al., 2016; Ayata et al., 2004) reports this decrease to be species dependent and usually either very small or even absent.

In our experiments the blood flow is modeled as a piecewise continuous function $q(t)$ of the form

$$q(t) = \begin{cases} q_0, & \text{for } t < t_1 \\ q_0\left(1+1.3\,\frac{t-t_1}{t_{r_1}}\right), & \text{for } t_1 < t < t_1+t_{r_1} \\ 2.3q_0, & \text{for } t_1+t_{r_1} < t < t_1+t_{r_1}+t_h \\ q_0\left(a\cdot e^{-\alpha(t-t_1-t_{r_1}-t_h)}+b\right), & \text{for } t_1+t_{r_1}+t_h < t < t_1+t_{r_1}+t_h+t_{r_2} \\ 0.7q_0, & \text{for } t > t_1+t_{r_1}+t_h+t_{r_2} \end{cases}$$

with $t_1 = t_i + t_d$, where t_i is the initial time of the first SD event, $t_d = 20$ seconds is the delay with respect to the onset of the SD

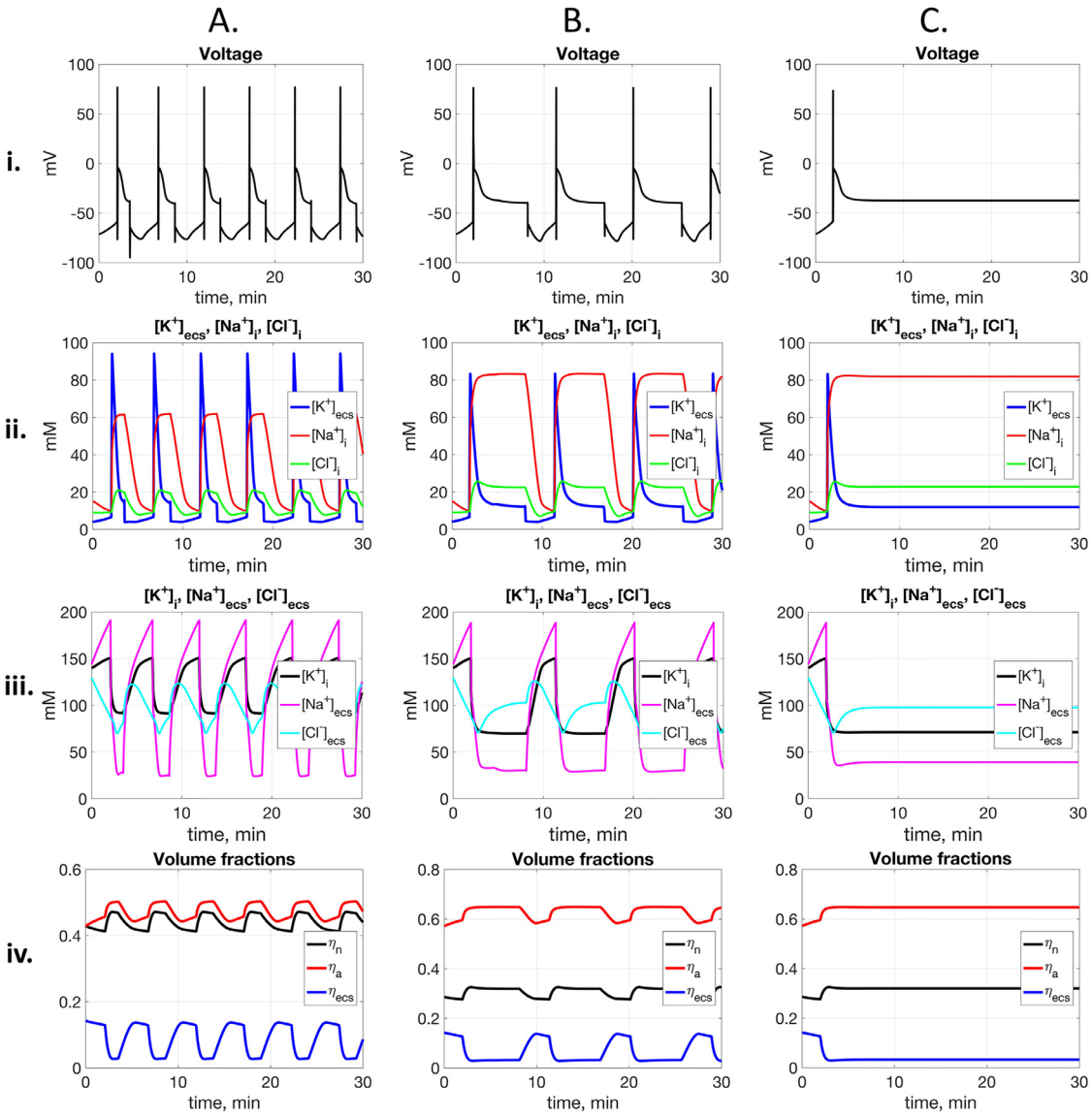

Fig. 2. Electrophysiological activity during cortical spreading depression. The membrane potential (i), the ionic concentrations of intracellular and extracellular sodium, potassium and chloride (ii, iii) and the variation over time in the volume fractions (iv) during SD for the two protocols: the left column A. shows the case for which the volume of the neuron equals the one of the astrocyte (Protocol A), while the middle column B. captures the case in which the astrocytic volume is two times larger than the neuronal one (Protocol B). Right column C shows the results for the SD electrophysiological activity when the metabolic response is not included in the model.

and q_0 denotes the baseline value of cerebral blood flow. The ramping times during which the blood flow increases and decreases are denoted by t_{r_1}, and t_{r_2} respectively, while t_h is the duration of the hyperemia; the values $a = 1.6298$ and $b = 0.6701$ were chosen so that the function $q(t)$ is continuous. Therefore, our blood flow protocol starts from baseline value $q = q_0$, rises by 130% for a short period of $t_h = 90$ seconds and then is followed by a slow decrease to 70% of its initial value. A complete list of the parameter values used in the computed examples can be found in Table 1.

4. Results and discussion

In the present article, the SD event is triggered by an increased ambient potassium concentration encoded in the diffusion flux through the concentration K_{bath}. This approach reproduces an experimental setting where the brain slices are perfused with a high potassium to provoke CSD and has been employed in multiple experimental and computational tests (Spong and Robertson, 2016; Cozzolino et al., 2018; Wei et al., 2014; Hübel et al., 2017; Florence et al., 2009). Alternative triggering mechanisms that were not considered here include oxygen-glucose deprivation, while keeping the potassium bath concentration at resting state value [38]. The time courses of membrane potential, ionic concentrations and volume fraction of the cells predicted by our model during the two different protocols are displayed in Fig. 2. The panels in the left refer to Protocol A, on the middle to Protocol B and on the right to the case in which the metabolic response was not taken into account and $\eta_a = 2\eta_n$.

In Protocol A, the model prediction shows 6 SD events during the 30 min simulation, as shown in panel A (i). The duration of the first event, which is accompanied by a hyperemic response, is of 85 seconds, while the duration of the subsequent SD waves, characterized by a mild hypoperfusion, increases to approximately 110 s.

At the onset of each cortical spreading depolarization, there is a short high frequency burst, with firing frequency reaching 250 Hz. This seizure-like episode lasts for approximately 0.1 s, followed by depolarization block. In order to better visualize this behavior,

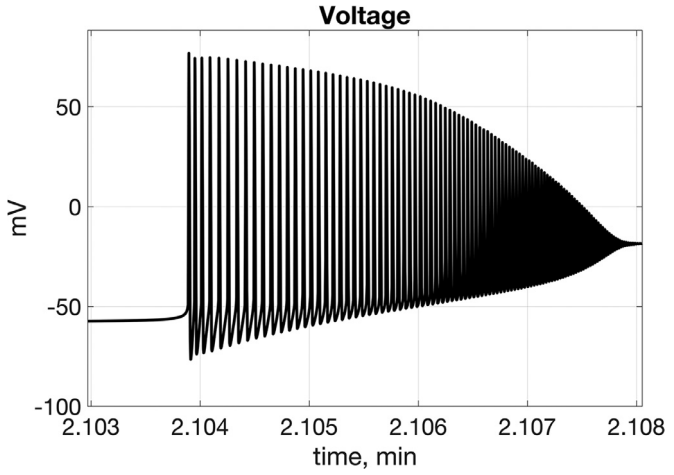

Fig. 3. Magnification of the time course of the membrane potential at the onset of the cortical spreading depolarization event.

Fig. 3 shows a magnification at time t = 2 min of the membrane potential.

To understand better the role of the metabolism, consider first the purely electrophysiological simulation of column C in Fig. 2. The presence of glutamate in the cleft results in the opening of the ion channels, leading to the initial increase in intraneural sodium. The neuron firing starts as a normal firing, but quickly the depolarization block due to the elevated extracellular potassium concentration fed by the diffusion term ensues. As the astrocytes are not capable of clearing the potassium to normal levels, the membrane voltage potential prevents the repolarization and normal firing. After the firing episode, intracellular sodium and extracellular potassium stabilize at abnormally high levels, corresponding to the depolarization, or depressed state of the neuron.

Consider now the results shown in columns A and B of Fig. 2, where the metabolic coupling has been introduced. The description is basically the same as without metabolism. However, as the bursting event consumes ATP both in neuron and astrocyte, the phosphorylation states p_a and p_n fall significantly below normal levels, meaning that both the pump current I_{pump} and cleaning current I_{glia} are lower than in the purely electrophysiological simulation. While the plateauing values of the electrolytes are similar in both cases, in the case with the metabolic coupling the equilibrium is reached with lower flux values. When the ATP supply in the cells returns to normal values, there is a sudden increase in the phosphorhylation states p_n and p_a and consequently in both I_{pump} and I_{glia}, accompanied by a swift decrease in intracellular sodium and extracellular potassium. The system is driven close to normal levels, and the process restarts again.

In the literature, the astrocytes have been suggested to have a neuroprotective role in SD events. Seidel et al. (2016); Lian and Stringer (2004) and Tamura et al. (2012). While the effect on neurons in our simulation is not clear, it is of interest to point out that as shown in panel B (i) of Fig. 2, the total number of SD waves recorded during the 30 min simulation period decreases from six to three, with a clear increase in duration, 370 s for the first SD episode, and 330 for the following ones.

In both protocols there are large variations in the ionic concentrations of sodium, potassium and chloride, as shown in the second and third row of Fig. 2. Our model predictions capture the typical electrophysiological signature of the depolarization epochs (Ayata and Lauritzen, 2015; Nedergaard and Hansen, 1993; Somjen, 2001), comprising a significant increase in the concentration of extracellular potassium and intracellular sodium (see Fig. 2, A (ii) and B (ii)) accompanied by a decrease in the concentration of intracellular potassium and extracellular sodium (see Fig. 2, A (iii) and B (iii)). Intracellular chloride concentration exhibits a small increase, while the extracellular chloride concentration shows a more significant decay. The large differences between the two protocols are in the potassium concentration. In agreement with the literature (Ayata and Lauritzen, 2015; Nedergaard and Hansen, 1993; Somjen, 2001) and in support of the potassium clearing role of astrocytes, in the case of a larger astrocytic volume (Protocol B), the concentration of extracellular potassium reaches 80 mM during the depression episode, while under Protocol A, it tops at 93 mM. Similarly, the intracellular sodium concentration increases to 80 mM during Protocol B, while reaching only 60 mM in Protocol A.

The bottom panels of Fig. 2 show that our model can follow the extreme morphologic changes which take place during the passing of the depolarization waves, in agreement with recent experimental literature reporting a significant 50–78% shrinkage of the extracellular space and swelling of the cellular compartments (Takano and Nedergaard, 2009; Cozzolino et al., 2018; Mazel et al., 2002; 1998). Our model predicts a 77% decrease in the volume fraction of the extracellular space, a 14% increase in the volume fraction of the astrocyte and a 16% increase in the neuron, well within the range suggested by the literature (Mazel et al., 2002; 1998; Kager et al., 2000).

4.1. Importance of the electro-metabolic coupling in SD studies

The double feedback mechanism coupling electrophysiology and metabolism is essential to fully understand the complexity of the spreading depolarization phenomenon, and how the concerted metabolic action of neurons and astrocytes regulates the brain electrical activity. To underline the importance of metabolism in spreading depression, we ran Protocol B uncoupling metabolism from electrophysiology. The results, shown in Fig. 2 column C, are rather different from the experimental observation. In fact, under the same conditions we now have a single SD event, thus without accounting for the metabolic contribution the model is unable to reproduce spontaneously consecutive events. This further confirms that the SD waves are indeed the outcome of the complex interplay between electrophysiology, metabolism and hemodynamics, and cannot be completely understood without this coupling.

The details of the metabolic response to the SD conditions under Protocol A (rows A1 and A2) and Protocol B (rows B1 and B2) are shown in Fig. 4. Glucose concentrations under Protocol A (panel A1 (i)) exhibit a steep decay in all the compartments, a behavior which has been observed and analyzed in several recent experimental reports (Ayata and Lauritzen, 2015; Feuerstein et al., 2010; Hashemi et al., 2009; Hoffmann et al., 2013). During the first depolarization event, glucose concentrations in neuron and extracellular space decrease by 58%, after which they recover reaching up to 81% of the resting state value by the time the next SD event starts. During the second SD event, which is no longer accompanied by large hyperemia, but instead occurs while the blood flow is 30% below baseline, there is an even larger decrease in glucose concentrations, by up to 68% of the initial values. In each subsequent SD event, glucose concentrations continue to decrease slightly, falling by 69% below baseline values in the sixth SD wave. The decrease of glucose concentration in astrocyte is much more significant: during the first episode, our model predicts a decay of 85% of baseline, with additional decay during the following SDs, reaching a maximum decrease of 89% of baseline during the sixth SD episode. Glucose concentrations follow a similar pattern under Protocol B (see Fig. 4, B1 (i)) decreasing by 50% in neuron and extracellular space during the first SD events and continuing to decrease all the way to 70% below baseline at the end of the last event. As in Protocol A, the decay in astrocyte is even more

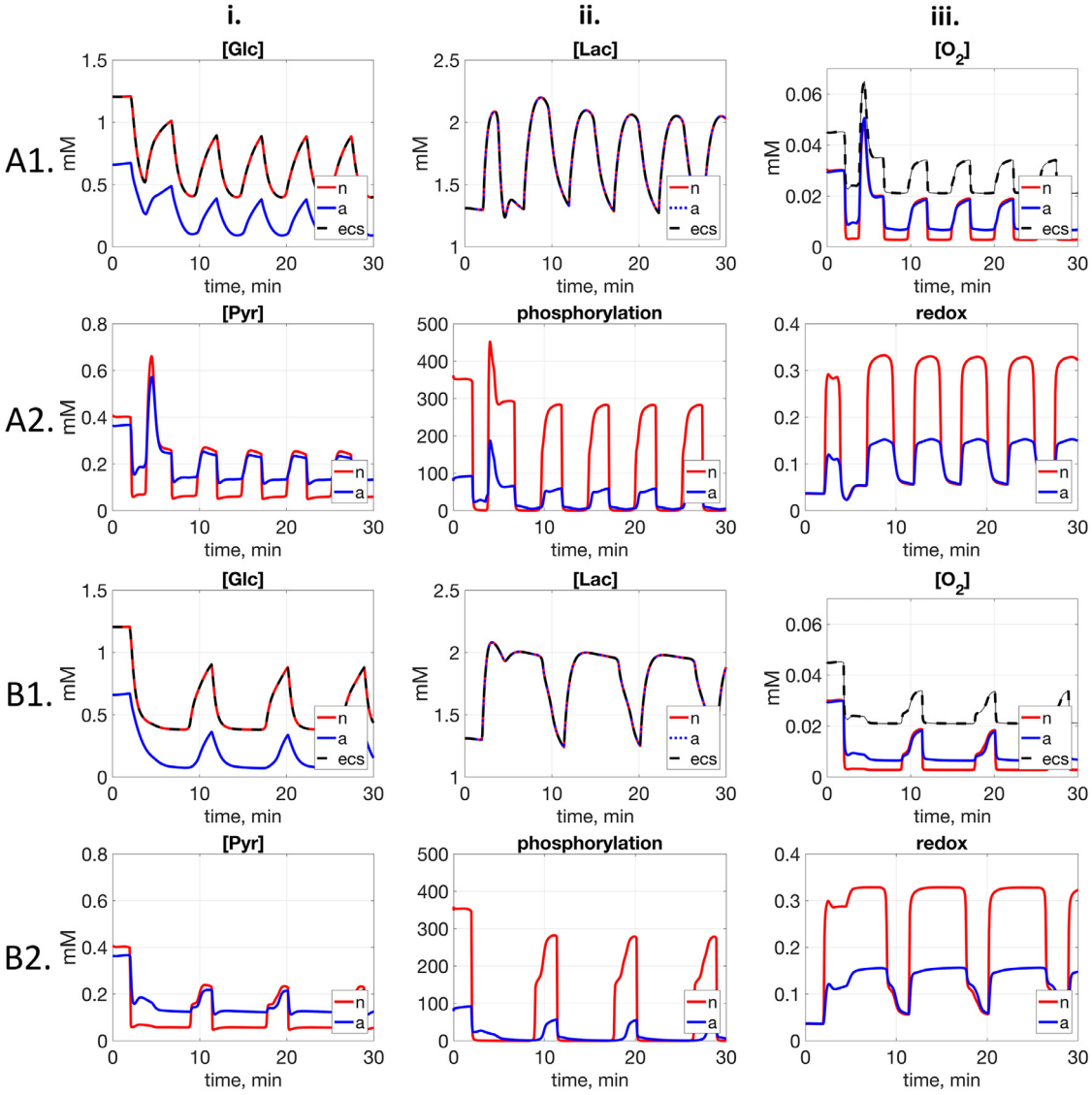

Fig. 4. Metabolic response to cortical spreading depression under Protocol A (rows A1 and A2) and Protocol B (rows B1 and B2). Concentration of glucose, lactate and oxygen in neuron (red), astrocyte (blue) and extracellular space (black). Concentration of pyruvate in neuron (red) and astrocyte (blue), phosphorylation state (A2 (ii) and B2 (ii)) in neuron (red) and astrocyte (blue) and redox states (A2 (iii) and B2 (iii)) in neuron (red) and astrocyte (blue). (For interpretation of the references to colour in this figure legend, the reader is referred to the web version of this article.)

pronounced, up to 60% during the passing of the first wave, and to 90% below baseline during the last event.

Lactate concentrations in neuron, astrocyte and extracellular space exhibit an increase of 65% above baseline during the first cortical spreading depression wave and an even greater increase of approximately 70% in the subsequent waves. These predictions are in agreement with recent experimental literature, reporting the extracellular lactate increase between 63% (Feuerstein et al., 2016) and 80% (Mies and Paschen, 1984; Selman et al., 2004).

The third panel A1 (iii) in the first row shows that in extracellular space, oxygen decreases by 50% during the first wave, after which it rapidly tops to 44% above its initial value. The second SD episode is accompanied by a stronger decrease in oxygen concentration, 54% below baseline, followed by slightly further decreases in each successive episode. In astrocyte, the decrease in oxygen concentration is much more significant: 69% of baseline during the first event, and 80% in the second one. The largest depletion of oxygen, however, is observed in neuron, where it drops by 90% of its resting state value in the first episode and slowly continues to decrease with each subsequent one, up to maximum decay of 93% in the case of the last wave, in line with the literature (Ayata and Lauritzen, 2015; Takano and Nedergaard, 2009; Takano et al., 2007).

The panels in the second and forth row of Fig. 4 (A2 (i) and B2 (i)), show the depletion of pyruvate during each wave. In Protocol A, pyruvate concentration shows a pronounced overshoot once the first depolarization event ends, 65% above baseline in neuron and 57% above baseline value in astrocyte, unlike in Protocol B, where instead of an overshoot, we see the concentration of pyruvate recovering to approximately 70% of its initial value. The significant energetic demand induced by the SD can be observed in Fig. 4, panels A2 (ii) and B2 (ii), where we see a 99% drop in phosphorylation state in the neuron and a 75% drop in astrocyte, with an even more dramatic reduction during the second SD wave where the decreases reach 99.5% in neuron and 97.5% in astrocyte, respectively. A similar pattern in phosphorylation state can be observed in Protocol B.

The increased metabolic cost of the passing SD events can be observed also in redox states in Fig. 4 (A2 (iii) and B2 (iii)), exhibiting a 4-fold increase in astrocyte and 10-fold increase in neuron.

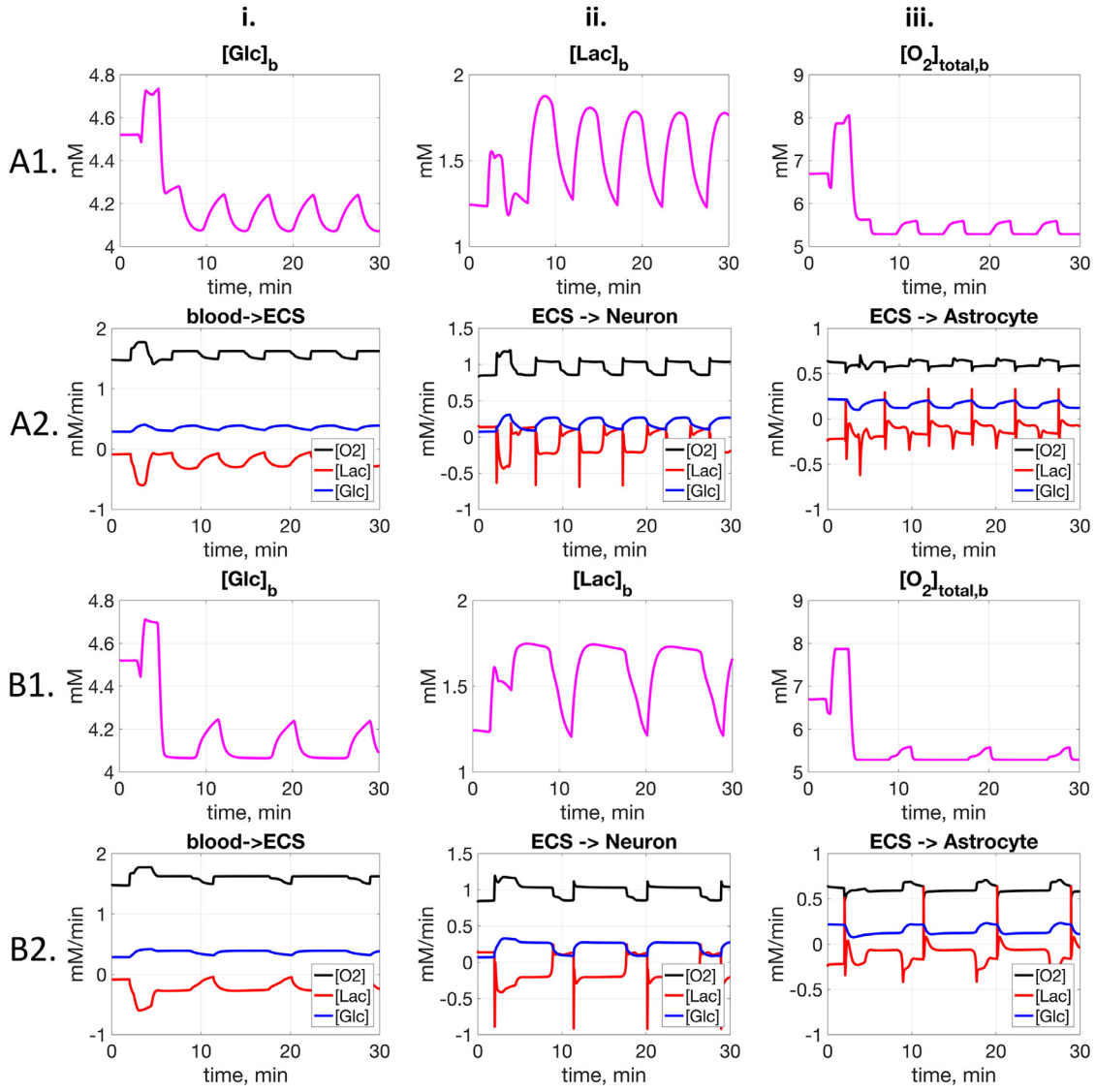

Fig. 5. Metabolic response in the blood compartment during the passing of multiple cortical spreading depression waves. The first two rows (A1 and A2) correspond to Protocol A, for which $\eta_n = \eta_a$, while the following two rows (B1 and B2) show the results obtained under Protocol B, where the glial volume is twice the neuronal volume. Rows A1 and B1 show the concentrations of glucose, lactate and oxygen in the blood compartments, while rows A2 and B2 display the transport fluxes of these three metabolites between blood and extracellular space, extracellular space and neuron, and extracellular space and astrocyte, respectively.

Due to the initial hyperemia, the first rise in the redox state is slightly lower compared to the redox state during the following SD waves.

Fig. 5 shows the time course of the concentrations of glucose, lactate and oxygen in blood and the transport fluxes of these three metabolites between different compartments. Under both protocols we observe that the large hyperemia produces, as expected, an initial increase in glucose and oxygen concentration: 4.5% and 19%, respectively, over resting state values. Once hyperemia subsides and vasoconstriction begins, the passing cortical spreading depression waves cause a decay of approximately 5% in glucose and 16% in oxygen concentration compared to initial values. During the first SD wave, the hyperemia induced oxygen surplus limits the increase in lactate to 23%, while in the following waves, as the availability of oxygen is reduced, lactate production increases to 53% of baseline. The transport fluxes in rows A2 and B2 show an increase of up to 25% above baseline in the transport of oxygen between blood and ecs during the first wave, and of approximately 14% during the following ones. Similarly, the glucose flux between blood and ecs shows an increase of 43% above baseline, while lactate exhibits an 8-fold decrease during the passing of the first wave, followed by a 4-fold decrease for the following SD waves. Similarly, the transport rate of oxygen from ecs to neuron increases 40% above the resting state value in the first event and 29% during the next ones, in agreement with the literature (Ayata and Lauritzen, 2015; Fordsmann et al., 2013) while the transport rate of glucose exhibits a 4-fold increase. The flux of lactate between ecs and neuron decreases 3-fold and exhibits a shift in direction, indicating that during SD events lactate is shuttled from neuron to extracellular space, unlike in resting state, when lactate is transported from ecs into neuron. The lactate flux between ecs and astrocyte, however, starts at a negative value as lactate leaves astrocyte, changes direction for a brief period at the onset of each SD event, showing a brief 6-fold increase above baseline, after which it changes direction again, remaining negative throughout the passing of the consecutive waves, indicating that astrocyte continues to efflux lactate.

Fig. 6 displays the time course of the reaction fluxes predicted by the model. The first plot in the first row shows that the flux of glycolysis under Protocol A in neuron has a large increase during the first event, about 7.5-fold of baseline value, subsequently

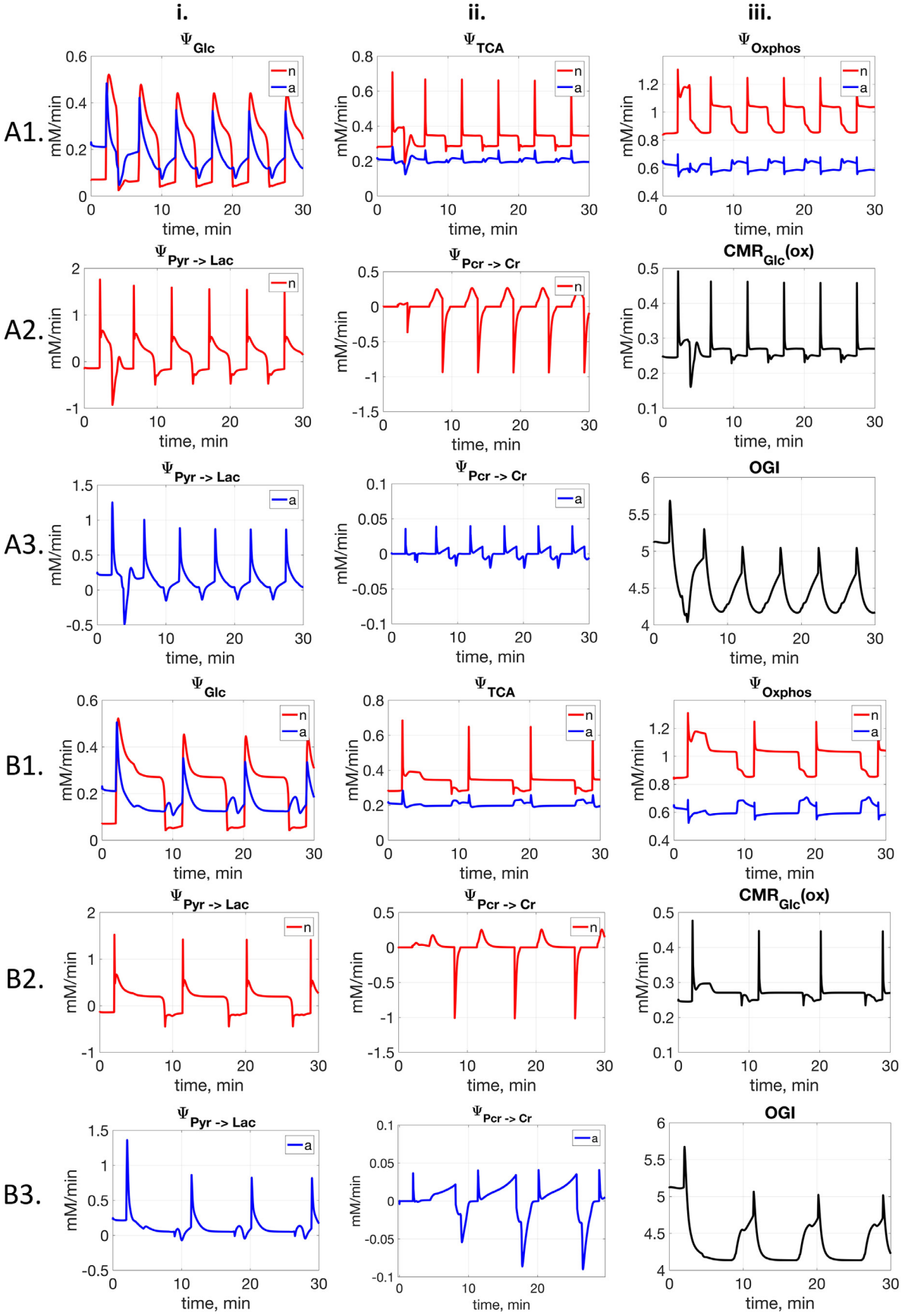

Fig. 6. Reaction fluxes for the electro-metabolic CSD model. The panels in rows A1, A2 and A3 show the reaction fluxes corresponding to Protocol A, while those in rows B1, B2 and B3 display the fluxes under Protocol B. Rows A1 and B1 Left to right: glycolysis flux (i), tricarboxylic acid cycle flux (ii) and oxidative phosphorylation (iii). Rows A2. and B2. Left to right: lactate dehydrogenase balance flux for neuron (i), creatine phosphorylation flux for neuron (ii), cerebral metabolic rate of glucose oxidation (iii), Rows A3 and B3. Left to right: lactate dehydrogenase balance flux for astrocyte (i), creatine phosphorylation flux for astrocyte (ii) and oxygen glucose index (iii).

decreasing to 6.7-fold for the second event and continuing to decrease to a 6-fold decrease during the last wave. In astrocyte, an 86% increase above baseline value at the onset of the first SD event is observed, followed by a 75% decrease below baseline. At the beginning of the second wave, glycolysis rate in astrocyte has recovered to 85% of its initial value, prior to the next less significant increase of 52% over baseline, followed again by a decrease. Panel A1 (ii) shows the TCA fluxes which exhibit a large overshoot at the beginning of each SD event: up to 240% of baseline value in neuron and 25% in astrocyte. Similarly, the oxidative phosphorylation flux in neuron rises by 53% for the first few seconds of the first SD wave, after which it stabilizes around 39% above its resting state value, and is then followed by smaller increases during subsequent next waves. In astrocyte, on the other hand, the oxidative phosphorylation flux decreases to 83% of its baseline value. In neuron, the lactate dehydrogenase flux changes direction during the SD wave, when lactate is transformed into pyruvate at a very large rate, while in the astrocyte the direction change occurs for a brief period only at the end of each passing wave. The creatine phosphorylation fluxes in neuron and astrocyte increase during the SD event, followed by a large decrease and a shift in direction at the end of each passing wave for a very brief period when phosphocreatine is transformed into creatine. The oxygen glucose index displayed in panels A3 (iii) and B3 (iii), defined as the ratio of the oxygen and glucose fluxes from blood to extracellular space, starts at a resting value of 5.15, and exhibits a very brief initial increase at the onset of the depolarization wave, followed by a strong decrease to approximately 4.

4.2. Effect of increasing the volume of the glial compartment

Glial cells have been actively studied in recent years, as increasing evidence points towards their essential role in the brain (Attwell et al., 2010). In particular, in the context of cortical spreading depression, astrocytes are in charge of clearing the extracellular potassium and glutamate, (Seidel et al., 2016; Fujita et al., 2015; Tamura et al., 2012) regulating the cerebral blood flow (Seidel et al., 2016; Filosa et al., 2016; Attwell et al., 2010) and the extracellular space ionic composition, size and geometry (Rovegno and Saez, 2017; Syková and Chvátal, 2000). Various literature contributions suggest that regions of brain with a higher number of glial cells, in particular astrocytes, are less susceptible to SD (Ayata and Lauritzen, 2015; Seidel et al., 2016; Karunasinghe and Lipski, 2013; Kager et al., 2000; Pomper et al., 2006; Funke et al., 2009). In addition, Fujita et al. (2015) demonstrated a direct correlation between the density of astrocytes and the propagation speed of the SD waves, which slow down in regions with a large number of astrocytes. The predictions of the model under Protocol B are in full agreement with the results in the literature. In Fig. 2 we observe a lower increase in the potassium extracellular concentration for Protocol B, as it is cleared by the larger number of astrocytes. Also, the duration of the cortical spreading depression events is longer during Protocol B: 370 s compared to 85 s for the first SD wave in Protocol A and 330 s compared to 110 s for the following SD waves. For the metabolism, under Protocol B we observe a lower increase in glycolysis and TCA than during Protocol A (See Fig. 6), which is not surprising because of the larger availability of the ATP shown in Fig. 4. Moreover, the LDH1 flux and the creatine phosphorylation flux in neuron, as well as the oxidative cerebral metabolic rate of glucose, are lower in the case of larger astrocytic volume.

To fully understand how increased astrocytic density affects the frequency, duration and intensity of SD waves, several extensions and refinements of the model are necessary. In our computer simulation, the environmental effectors that trigger SD events are modeled as a diffusion current involving the ambient potassium concentration K_{bath}. In a spatially distributed model that can account for diffusion through neuron/astrocyte units, it is plausible that between SD bursts, the potassium levels are closer to normal than in the current model. Hence, while our spatially lumped model shows a change in the characteristics of the SD waves in connection with increased volume fraction of astrocyte, it does not provide a definite answer as to whether this translates into a neuroprotective role of astrocytes. In addition to lacking a spatial component, other potentially crucial factors missing in our model are astrocytic potassium siphoning into the blood flow through the end feet and a detailed description of glutamate-glutamine cycling between astrocytes and neurons. A recent paper Conte et al. (2018) proposes a model including a detailed description of the Na^+-glutamate transporter and consider the role of elevated glutamate and potassium concentration in the triggering, propagation and recurrence of SD events. We will revisit this question with an extension our model that includes these factors in future work.

Acknowledgments

This work was partly supported by the Basque government through BERC 2018–2021, the Spanish Ministry of Economics and Competitiveness MINECO through BCAM Severo Ochoa excellence accreditation SEV-2017-0718 and the “Plan Estatal de Investigación Desarollo e Innovación Orientada a los Retos de la Sociedad” under Grant BELEMET - Brain ELEctro-METabolic modeling and numerical approximation (MTM2015-69992-R), and the Spanish State Research Agency (AEI/FEDER) under grant MULTIQUANT - MULTIscale modeling with applications in QUANTitative bioscience (RTI2018-093416-B-I00). The work of Daniela Calvetti was partly support by NSF grants DMS-1522334 and NIH grant 1U01 GM111251-01. The work of Erkki Somersalo was partly support by NSF grants DMS 1714617 and NIH grant 1U01 GM111251-01.

References

Adachi, K., Cruz, N.F., Sokoloff, L., Dienel, G.A., 1995. Labeling of metabolic pools by [6-14c] glucose during k+-induced stimulation of glucose utilization in rat brain. J. Cerebral Blood Flow Metabol. 15 (1), 97–110.
Attwell, D., Buchan, A.M., Charpak, S., Lauritzen, M., MacVicar, B.A., Newman, E.A., 2010. Glial and neuronal control of brain blood flow. Nature 468 (7321), 232.
Ayata, C., Lauritzen, M., 2015. Spreading depression, spreading depolarizations, and the cerebral vasculature. Physiol. Rev. 95 (3), 953–993.
Ayata, C., Shin, H.K., Salomone, S., Ozdemir-Gursoy, Y., Boas, D.A., Dunn, A.K., Moskowitz, M.A., 2004. Pronounced hypoperfusion during spreading depression in mouse cortex. J. Cerebral Blood Flow Metabol. 24 (10), 1172–1182.
Balança, B., Meiller, A., Bezin, L., Dreier, J.P., Marinesco, S., Lieutaud, T., 2017. Altered hypermetabolic response to cortical spreading depolarizations after traumatic brain injury in rats. J. Cerebral Blood Flow Metabol. 37 (5), 1670–1686.
Barreto, E., Cressman, J.R., 2011. Ion concentration dynamics as a mechanism for neuronal bursting. J. Biol. Phys. 37 (3), 361–373.
Bosche, B., Graf, R., Ernestus, R.-I., Dohmen, C., Reithmeier, T., Brinker, G., Strong, A.J., Dreier, J.P., Woitzik, J., 2010. Recurrent spreading depolarizations after subarachnoid hemorrhage decreases oxygen availability in human cerebral cortex. Ann. Neurol. 67 (5), 607–617.
Busija, D.W., Bari, F., Domoki, F., Horiguchi, T., Shimizu, K., 2008. Mechanisms involved in the cerebrovascular dilator effects of cortical spreading depression. Progress Neurobiol. 86 (4), 417–433.
Calvetti, D., Capo Rangel, G., Gerardo Giorda, L., Somersalo, E., 2018. A computational model integrating brain electrophysiology and metabolism highlights the key role of extracellular potassium and oxygen. J. Theoret. Biol. 446, 238–258.
Calvetti, D., Somersalo, E., 2011. Dynamic activation model for a glutamatergic neurovascular unit. J. Theoret. Biol. 274 (1), 12–29.
Capo Rangel, G., Prezioso, J., Gerardo-Giorda, L., Somersalo, E., Calvetti, D., 2019. Brain energetics plays a key role in the coordination of electrophysiological activity, metabolism and hemodynamics: evidence from an integrated computational model. J. Theor. Biol. 478, 26–39.
Carlson, A.P., Carter, R.E., Shuttleworth, C.W., 2012. Vascular, electrophysiological, and metabolic consequences of cortical spreading depression in a mouse model of simulated neurosurgical conditions. Neurol. Res. 34 (3), 223–231.
Charles, A.C., Baca, S.M., 2013. Cortical spreading depression and migraine. Nature Rev. Neurol. 9, 637–644.
Conte, C., Lee, R., Sarkar, M., Terman, D., 2018. A mathematical model of recurrent spreading depolarizations. J. Comput. Neurosci. 44 (2), 203–217.

Cozzolino, O., Marchese, M., Trovato, F., Pracucci, E., Ratto, G.M., Buzzi, M.G., Sicca, F., Santorelli, F.M., 2018. Understanding spreading depression from headache to sudden unexpected death. Frontiers in Neurol. 9, 19.
Cressman, J.R., Ullah, G., Ziburkus, J., Schiff, S.J., Barreto, E., 2009. The influence of sodium and potassium dynamics on excitability, seizures, and the stability of persistent states: i. single neuron dynamics. J. Comput. Neurosci. 26 (2), 159–170.
Dalkara, T., Zervas, N.T., Moskowitz, M.A., 2006. From spreading depression to the trigeminovascular system. Neurol. Sci. 27 (2), s86–s90.
Dreier, J.P., Major, S., Manning, A., Woitzik, J., Drenckhahn, C., Steinbrink, J., Tolias, C., Oliveira-Ferreira, A.I., Fabricius, M., Hartings, J.A., et al., 2009. Cortical spreading ischaemia is a novel process involved in ischaemic damage in patients with aneurysmal subarachnoid haemorrhage. Brain 132 (7), 1866–1881.
Feuerstein, D., Backes, H., Gramer, M., Takagaki, M., Gabel, P., Kumagai, T., Graf, R., 2016. Regulation of cerebral metabolism during cortical spreading depression. J. Cerebral Blood Flow Metabol. 36 (11), 1965–1977.
Feuerstein, D., Manning, A., Hashemi, P., Bhatia, R., Fabricius, M., Tolias, C., Pahl, C., Ervine, M., Strong, A.J., Boutelle, M.G., 2010. Dynamic metabolic response to multiple spreading depolarizations in patients with acute brain injury: an online microdialysis study. J. Cerebral Blood Flow Metabol. 30 (7), 1343–1355.
Filosa, J.A., Morrison, H.W., Iddings, J.A., Du, W., Kim, K.J., 2016. Beyond neurovascular coupling, role of astrocytes in the regulation of vascular tone. Neuroscience 323, 96–109.
Florence, G., Dahlem, A.M., Almeida, A.-C.G., Bassani, J., Kurths, J., 2009. The role of extracellular potassium dynamics in the different stages of ictal bursting and spreading depression: a computational study. J. Theoret. Biol. 258 (2), 219–228.
Fordsmann, J.C., Ko, R.W., Choi, H.B., Thomsen, K., Witgen, B.M., Mathiesen, C., Lønstrup, M., Piilgaard, H., MacVicar, B.A., Lauritzen, M., 2013. Increased 20-hete synthesis explains reduced cerebral blood flow but not impaired neurovascular coupling after cortical spreading depression in rat cerebral cortex. J. Neurosci. 33 (6), 2562–2570.
Fujita, S., Mizoguchi, N., Aoki, R., Cui, Y., Koshikawa, N., Kobayashi, M., 2015. Cytoarchitecture-dependent decrease in propagation velocity of cortical spreading depression in the rat insular cortex revealed by optical imaging. Cerebral Cortex 26 (4), 1580–1589.
Funke, F., Kron, M., Dutschmann, M., Müller, M., 2009. Infant brain stem is prone to the generation of spreading depression during severe hypoxia. J. Neurophysiol. 101 (5), 2395–2410.
Galeffi, F., Somjen, G.G., Foster, K.A., Turner, D.A., 2011. Simultaneous monitoring of tissue Po2 and nadh fluorescence during synaptic stimulation and spreading depression reveals a transient dissociation between oxygen utilization and mitochondrial redox state in rat hippocampal slices. J. Cerebral Blood Flow Metabol. 31 (2), 626–639.
Hadjikhani, N., Del Rio, M.S., Wu, O., Schwartz, D., Bakker, D., Fischl, B., Kwong, K.K., Cutrer, F.M., Rosen, B.R., Tootell, R.B., et al., 2001. Mechanisms of migraine aura revealed by functional mri in human visual cortex. Proc. Natl. Acad. Sci. 98 (8), 4687–4692.
Hashemi, P., Bhatia, R., Nakamura, H., Dreier, J.P., Graf, R., Strong, A.J., Boutelle, M.G., 2009. Persisting depletion of brain glucose following cortical spreading depression, despite apparent hyperaemia: evidence for risk of an adverse effect of Leao's spreading depression. J. Cerebral Blood Flow Metabol. 29 (1), 166–175.
Hoffmann, U., Sukhotinsky, I., Eikermann-Haerter, K., Ayata, C., 2013. Glucose modulation of spreading depression susceptibility. J. Cerebral Blood Flow Metabol. 33 (2), 191–195.
Horiguchi, T., Snipes, J.A., Kis, B., Shimizu, K., Busija, D.W., 2005. The role of nitric oxide in the development of cortical spreading depression-induced tolerance to transient focal cerebral ischemia in rats. Brain Res. 1039 (1–2), 84–89.
Hübel, N., Andrew, R.D., Ullah, G., 2016. Large extracellular space leads to neuronal susceptibility to ischemic injury in a na+/k+ pumps–dependent manner. J. Comput. Neurosci. 40 (2), 177–192.
Hübel, N., Dahlem, M.A., 2014. Dynamics from seconds to hours in hodgkin-huxley model with time-dependent ion concentrations and buffer reservoirs. PLoS Comput. Biol. 10 (12), e1003941.
Hübel, N., Hosseini-Zare, M.S., Žiburkus, J., Ullah, G., 2017. The role of glutamate in neuronal ion homeostasis: a case study of spreading depolarization. PLoS Comput. Biol. 13 (10), e1005804.
Hübel, N., Ullah, G., 2016. Anions govern cell volume: a case study of relative astrocytic and neuronal swelling in spreading depolarization. PloS One 11 (3), e0147060.
Kager, H., Wadman, W.J., Somjen, G.G., 2000. Simulated seizures and spreading depression in a neuron model incorporating interstitial space and ion concentrations. J. Neurophys. 84 (1), 495–512.
Karunasinghe, R.N., Lipski, J., 2013. Oxygen and glucose deprivation (ogd)-induced spreading depression in the substantia nigra. Brain Res. 1527, 209–221.
Kudo, C., Nozari, A., Moskowitz, M.A., Ayata, C., 2008. The impact of anesthetics and hyperoxia on cortical spreading depression. Exper. Neurol. 212 (1), 201–206.
Lauritzen, M., Dreier, J.P., Fabricius, M., Hartings, J.A., Graf, R., Strong, A.J., 2011. Clinical relevance of cortical spreading depression in neurological disorders: migraine, malignant stroke, subarachnoid and intracranial hemorrhage, and traumatic brain injury. J. Cerebral Blood Flow Metabol. 31 (1), 17–35.
Lauritzen M, T.W., J, O., 1981. Eeg during attacks of common and classical migraine. Cephalalgia 1, 63–66.
Leão, A.A.P., 1944. Spreading depression of activity in the cerebral cortex. J. Neurophysiol. 7, 359–390.
Leão, A.A.P., 1945. Propagation of spreading depression. J. Neurophysiol. 8, 33–45.
Lian, X.-Y., Stringer, J.L., 2004. Energy failure in astrocytes increases the vulnerability of neurons to spreading depression. Eur. J. Neurosci. 19 (9), 2446–2454.
Lourenço, C.F., Ledo, A., Gerhardt, G., Barbosa, R.M., 2017. Nneurometabolic and electrophysiological changes during cortical spreading depolarization: multimodal approach based on a lactate-glucose dual microbiosensor arrays. Scientific Reports 7 (1), 6764.
Masamoto, K., Kanno, I., 2012. Anesthesia and the quantitative evaluation of neurovascular coupling. J. Cerebral Blood Flow Metabol. 32 (7), 1233–1247.
Mazel, T., Richter, F., Vargová, L., Syková, E., 2002. Changes in extracellular space volume and geometry induced by cortical spreading depression in immature and adult rats. Physiol. Res. 51, S85–S94.
Mazel, T., Sĭmonová, Z., Syková, E., 1998. Diffusion heterogeneity and anisotropy in rat hippocampus. Neuroreport 9 (7), 1299–1304.
Mies, G., Paschen, W., 1984. Regional changes of blood flow, glucose, and atp content determined on brain sections during a single passage of spreading depression in rat brain cortex. Exper. Neurol. 84 (2), 249–258.
Nedergaard, M., Hansen, A.J., 1988. Spreading depression is not associated with neuronal injury in the normal brain. Brain Res. 449 (1–2), 395–398.
Nedergaard, M., Hansen, A.J., 1993. Characterization of cortical depolarizations evoked in focal cerebral ischemia. J. Cerebral Blood Flow Metabol. 13 (4), 568–574.
Piilgaard, H., Lauritzen, M., 2009. Persistent increase in oxygen consumption and impaired neurovascular coupling after spreading depression in rat neocortex. J. Cerebral Blood Flow Metabol. 29 (9), 1517–1527.
Pomper, J.K., Haack, S., Petzold, G.C., Buchheim, K., Gabriel, S., Hoffmann, U., Heinemann, U., 2006. Repetitive spreading depression-like events result in cell damage in juvenile hippocampal slice cultures maintained in normoxia. J. Neurophys. 95 (1), 355–368.
Rogers, M.L., Feuerstein, D., Leong, C.L., Takagaki, M., Niu, X., Graf, R., Boutelle, M.G., 2013. Continuous online microdialysis using microfluidic sensors: dynamic neurometabolic changes during spreading depolarization. ACS Chemical Neurosci. 4 (5), 799–807.
Rovegno, M., Saez, J.C., 2017. Role of astrocyte connexin hemichannels in cortical spreading depression. Biochimica et Biophysica Acta (BBA)-Biomembranes.
Seidel, J.L., Escartin, C., Ayata, C., Bonvento, G., Shuttleworth, C.W., 2016. Multifaceted roles for astrocytes in spreading depolarization: a target for limiting spreading depolarization in acute brain injury? Glia 64 (1), 5–20.
Selman, W.R., Lust, W.D., Pundik, S., Zhou, Y., Ratcheson, R.A., 2004. Compromised metabolic recovery following spontaneous spreading depression in the penumbra. Brain Res. 999 (2), 167–174.
Somjen, G.G., 2001. Mechanisms of spreading depression and hypoxic spreading depression-like depolarization. Physiol. Rev. 81 (3), 1065–1096.
Spong, R.D.A., Kristin, E., Robertson, R.M., 2016. Mechanisms of spreading depolarization in vertebrate and insect central nervous systems. J. Comput. Neurophys. 116 (3), 1117–1127.
Syková, E., Chvátal, A., 2000. Glial cells and volume transmission in the CNS. Neurochem. Int. 36 (4–5), 397–409.
Takano, T., Nedergaard, M., 2009. Deciphering migraine. J. Clinical Invest. 119 (1), 16–19.
Takano, T., Tian, G.-F., Peng, W., Lou, N., Lovatt, D., Hansen, A.J., Kasischke, K.A., Nedergaard, M., 2007. Cortical spreading depression causes and coincides with tissue hypoxia. Nature Neurosci. 10 (6), 754.
Tamura, Y., Eguchi, A., Jin, G., Sami, M.M., Kataoka, Y., 2012. Cortical spreading depression shifts cell fate determination of progenitor cells in the adult cortex. J. Cerebral Blood Flow Metabol. 32 (10), 1879–1887.
Ullah, G., Wei, Y., Dahlem, M.A., Wechselberger, M., Schiff, S.J., 2015. The role of cell volume in the dynamics of seizure, spreading depression, and anoxic depolarization. PLoS Comput. Biol. 11 (8), e1004414.
Wei, Y., Ullah, G., Schiff, S.J., 2014. Unification of neuronal spikes, seizures, and spreading depression. J. Neurosci. 34 (35), 11733–11743.